Nanoscale structural evolution of electrically driven insulator to metal transition in vanadium dioxide

Eugene Freeman,[1,a)] Greg Stone,[2] Nikhil Shukla,[1] Hanjong Paik,[3] Jarrett A. Moyer,[4] Zhonghou Cai,[5] Haidan Wen,[5] Roman Engel-Herbert,[2] Darrell G. Schlom,[3,6] Venkatraman Gopalan,[2] and Suman Datta[1]

[1]*Department of Electrical Engineering, Pennsylvania State University, University Park, Pennsylvania 16802, USA*
[2]*Department of Materials Science and Engineering, Pennsylvania State University, University Park, Pennsylvania 16802, USA*
[3]*Department of Materials Science and Engineering, Cornell University, Ithaca, New York 14853, USA*
[4]*Department of Physics and Frederick Seitz Materials Research Laboratory, University of Illinois at Urbana-Champaign, Urbana, Illinois 61801, USA*
[5]*Advanced Photon Source, Argonne National Laboratory, Argonne, Illinois 60439, USA*
[6]*Kavli Institute at Cornell for Nanoscale Science, Ithaca, New York 14853, USA*

(Received 6 November 2013; accepted 9 December 2013; published online 30 December 2013)

The structural evolution of tensile strained vanadium dioxide thin films was examined across the electrically driven insulator-to-metal transition by nanoscale hard X-ray diffraction. A metallic filament with rutile (R) structure was found to be the dominant conduction pathway for an electrically driven transition, while the majority of the channel area remained in the monoclinic M1 phase. The filament dimensions were estimated using simultaneous electrical probing and nanoscale X-ray diffraction. Analysis revealed that the width of the conducting channel can be tuned externally using resistive loads in series, enabling the M1/R phase ratio in the phase coexistence regime to be tuned. © *2013 AIP Publishing LLC*.
[http://dx.doi.org/10.1063/1.4858468]

Transition metal oxides exhibit unique electronic properties, such as metal-insulator transition (MIT),[1] colossal magnetoresistance,[2] and superconductivity,[3] some of which are associated with correlated phase transitions as well as structural transitions. One such material of interest is vanadium dioxide (VO_2), which shows a complex interaction between the crystal structure and electronic properties. Depending on the temperature and strain, VO_2 supports three stable states, two insulating monoclinic (M1 and M2) and a metallic rutile (R) phase, along with a metastable triclinic (T) phase and a complex triple point.[4] Several models have been proposed to explain the MIT in VO_2,[5–10] attributing it to varying levels of contribution from a Mott-Hubbard type phase transition and a Peierls-like structural instability. Significant research efforts are geared towards a better understanding of the phase transition mechanisms in VO_2 to elucidate which description is most accurate. Recent work has provided evidence that an electrically driven MIT in VO_2 can be achieved in the monoclinic phase without a change in the crystal symmetry, hinting at the possibility of an experimental observation of a Mott transition without a Peierls-like structural phase transition,[11] enabled by the Mott M2 phase.[12]

Unlike a thermally driven MIT, the formation and growth of a filament plays an important role in an electrically driven MIT.[13–16] However, no conclusive evidence exists regarding the underlying crystal structure of this filament. In this work, the structural properties of the filament created during an electrically driven MIT in VO_2 thin films are investigated by nanoscale hard X-ray diffraction (XRD) spatial mapping. The structural evolution of the film and the geometric dimensions of the filament were measured as a function of the applied electric field.

The VO_2 films investigated were 10-nm-thick on semi-insulating TiO_2 (001) substrates, and grown by employing reactive oxide molecular-beam epitaxy using a Veeco GEN10 system.[17] The 0.9% lattice mismatch between the R-phase VO_2 and the (001) surface of a R-phase TiO_2 substrate results in commensurate VO_2 films having a shortened out-of-plane spacing (along the c-axis).[18,19] Two-terminal test structures were fabricated using standard lithographic techniques. Electrical contacts were patterned on the VO_2 surface using electron beam lithography and a 20-nm-thick Pd/80-nm-thick Au metal stack was deposited in the defined patterns by electron beam evaporation, followed by lift-off. The active channel and device isolation was then patterned by electron beam lithography followed by a CF_4 dry etch and residual e-beam resist was stripped with a 70 °C bath of Remover 1165. Finally, the sample was mounted on a ceramic package and device electrodes were wire-bonded to external leads. A scanning electron micrograph of the device is shown in Fig. 1(a). A 38 kΩ resistor was placed in series with the device to limit the current flowing through the film during the electrically induced transition. I-V measurements done at 260 K showed that the device with the series resistor transitioned from a high resistance state (HRS) to a low resistance state (LRS) at 9.6 V.

The structure of the VO_2 film as it transformed from the HRS to LRS was investigated using the nanoscale scanning X-ray probe at the 2-ID-D beamline at the Advanced Photon Source at Argonne National Laboratory. A 10.1 keV hard X-ray probe with a spot size as small as 250 nm

a)Electronic mail: exf181@psu.edu.

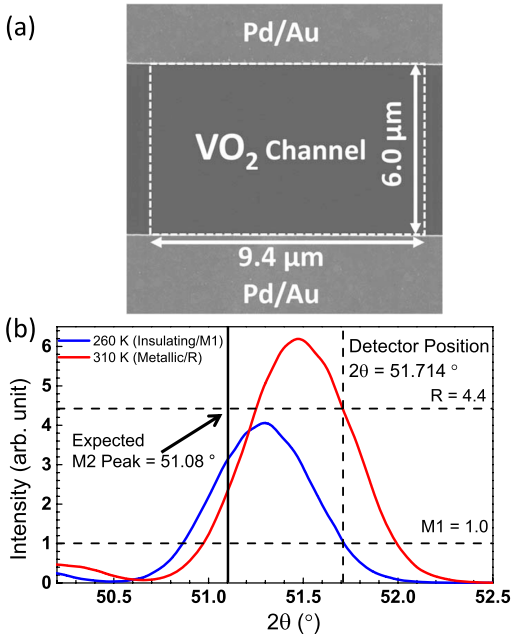

FIG. 1. (a) Scanning electron micrograph of the fabricated device, measured to be 6.0 μm in length and 9.4 μm wide. (b) $\theta/2\theta$ scan at 310 K (red line) and 260 K (blue line) of the R 002 and M1 $40\bar{2}$ Bragg peaks, respectively. The expected position of the M2 040 Bragg peak is calculated to be 51.08°. A 2θ angle of 51.714° was chosen for the subsequent mapping to provide maximum contrast between the different VO_2 phases.

full-width-half-maximum was achieved by an Au Fresnel zone plate (1.6 μm thick, 160 μm diameter, 100 nm outer most zone width, 40 μm center disk, and 40 μm central beam stop) in conjunction with a 20 μm order sorting aperture. Two-dimensional (2D) structural maps of a VO_2 channel were obtained by raster scanning the device under the X-ray probe at a fixed $\theta/2\theta$ angle while simultaneously monitoring the intensity of the diffracted beam using a single avalanche photodiode detector as a function of applied voltages across the device and series resistor. A liquid nitrogen cryostream (Oxford UMC0060) was used to maintain the sample at the desired temperature. For beam intensities above 1 MW/m^2, it was found that the X-ray caused a permanent transition into the M1 phase. The MIT control in VO_2 with high energy radiation has been observed by other groups.[20] The exact X-ray beam intensity threshold and mechanism of this phenomenon is still being investigated. In our case, a lower intensity of 750 W/m^2 was achieved by inserting attenuation filters into the X-ray beam prior to the zone plate and defocusing the beam to a 1 μm diameter spot size on the sample. The device channel was scanned using 500 nm steps along the length of the channel (in the direction of the applied electric field) and in 300 nm steps along the width (transverse to the applied electric field), providing information in the nanoscale regime.

Figure 1(b) shows the R 002 and M1 $40\bar{2}$ Bragg peaks measured at 310 K and 260 K, respectively, on the VO_2 thin film, along with the expected location of the M2 040 peak. Due to the metastable nature of the triclinic phase, it is not considered in this analysis. A 2θ angle of 51.714° was selected to provide the maximum intensity contrast between the M1 and R phases. At this angle, an increase in intensity indicates the presence of the R phase while a decrease would signify the presence of the M2 phase, which may appear in an electrically driven MIT. Thermally driving the film across the transition while scanning $\theta/2\theta$ did not reveal any evidence of an M2 phase in agreement with the recently published VO_2 temperature-stress phase diagram.[4]

Nanoscale XRD maps were collected for a range of applied voltages both above and below the electronically driven MIT. Figure 2 shows the intensity maps for the device at 260 K, for 0, 8, 10, and 12 V bias applied to the VO_2 channel and 38 kΩ resistor in series ($V_{total} = V_{VO_2} + V_{resistor}$). To highlight the structural changes from the M1 phase for different applied voltages, the intensity of the XRD maps was normalized with respect to the M1 intensity. In Fig. 2, the green regions are diffraction signals from the M1 phase of VO_2, blue is where the VO_2 is etched out, and red areas represent R domains. Figure 2(a) shows that the VO_2 channel was mainly in the M1 phase (HRS) under zero bias condition except for a small R filament at the center of the channel. This filament is likely a remnant from previous electrically driven transitions (i.e., memory effect); however, repeatedly cycling the device across the MIT and rescanning the channel did not always result in an observable remnant filament. At 0 V, the total channel resistance was 95.6 kΩ and the device was in HRS. The small R filament did not significantly contribute to the in-plane conduction, but can act as a

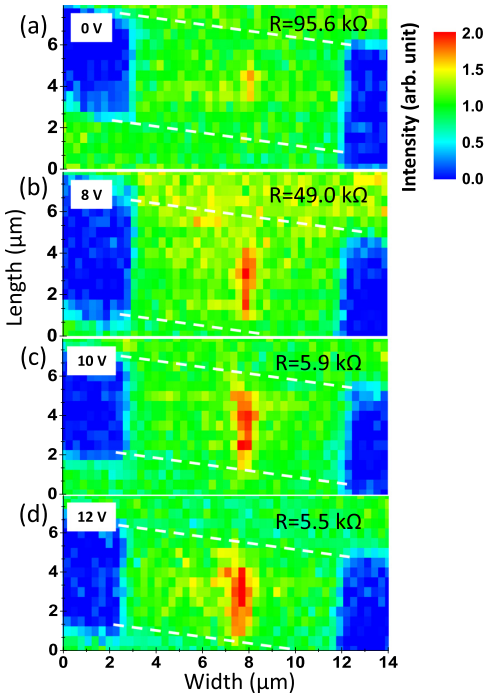

FIG. 2. 2 D nanoscale X-ray maps of a VO_2 device with applied voltages of (a) 0 V, (b) 8 V, (c) 10 V, and (d) 12 V with a series resistor of 38 kΩ, which shows the dynamical growth of an R-phase filament in the channel. Note in (a) that a remnant of the filament persisted when no voltage was applied across the channel. The white dashed lines represent the approximate edges of the gold electrodes.

shunting path for out of plane transport for vertical devices. For 8 V bias, a larger filament, approximately 3.2 μm long, was observed at the center, but did not bridge the entire channel, shown in Fig. 2(b). This filament at 8 V reduced the channel resistance by about half to 49.0 kΩ and forms before the device transitions to a LRS. Increasing the bias to 10 V, the VO_2 channel underwent an electrically driven transition into the LRS and the channel resistance dropped sharply to 5.9 kΩ. Figure 2(c) shows that in this state, the filament bridged the entire length of the 6 μm channel; however, its width is only a fraction of the lithographically defined 9.4 μm channel width. Finally, at 12 V applied voltage, the channel resistance was 5.5 kΩ, a 17x decrease from the equilibrium state at 0 V. The filament seen in Fig. 2(d) had a slightly increased width compared to the 10 V bias. At 12 V bias, the peak XRD intensity from the filament region was found to be only 2.1x (2.0x at 10 V bias) that of M1, which is significantly lower than the 4.4x expected increase observed in the bulk film for a thermally driven MIT. Assuming uniform X-ray illumination, this suggests that the filament occupied approximately 1/3 of the full 1 μm diameter beam size, indicating a filament width of approximately 300 nm. Additionally, no drop in intensity was observed in the channel that could be attributed to an M2 phase; as mentioned before this was expected from a tensile strained VO_2 film such as the one used in this experiment.

To confirm that the increased XRD intensity response was due to the MIT and to demonstrate repeatability, the diffraction intensity and the VO_2 resistance were simultaneously measured over several cycles of electrically induced transitions. A pulse train, shown in Fig. 3(a), was cycled from 1.3 V to 10 V, as 9.6 V was found to be sufficient to induce the electronic transition, while 1.3 V was low enough to return to an insulating state yet provide a finite current to confirm the resistance of the VO_2. The X-ray beam was focused on the conducting filament and the diffracted intensity was collected while simultaneously monitoring the channel resistance. Figures 3(b) and 3(c) shows that the LRS coincided with an increased intensity attributed to the R phase, whereas the HRS coincided with the M1 phase.

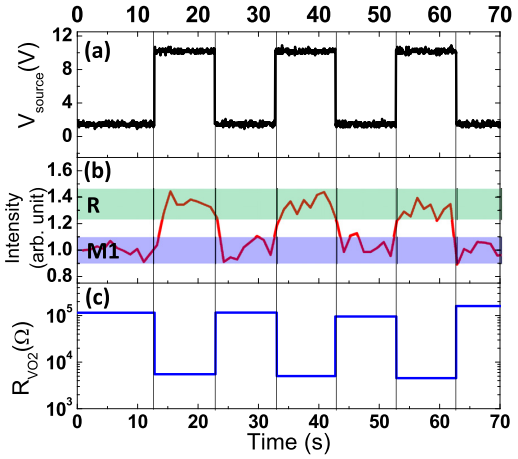

FIG. 3. (a) Voltage pulse applied to the VO_2 and 38 kΩ resistor in series. (b) The corresponding time dependent X-ray intensity from the filament region and (c) resistance of the entire channel. The changes in the X-ray intensity accompanied by changes in channel resistance are attributed to a structural phase transition in the VO_2 from the between the insulating M1 and metallic R phase.

To explain the difference in the channel resistivity change between the thermal (571x) and electrically (17x) driven transitions, the total resistance was calculated by incorporating the coexistence of low and high resistive phases. The channel was treated as a set of series and parallel resistors with the equivalent circuit diagram given in Fig. 4(a), overlaid on an illustration of an M1 channel with a rutile filament in the center. The total resistance of the equivalent circuit is given in Eq. (1) where R_{para-R} is the parallel resistor describing the rutile filament, $R_{series-M}$ and R_{para-M} are resistors with the resistivity characteristic of the monoclinic phase. $R_{series-M}$ components were combined into a single series resistor and similarly the R_{para-M} components were lumped into a single parallel resistor. ρ_M and ρ_R are the resistivities of the monoclinic and rutile phases, respectively; while *L, W, and t* are the length, width, and thickness of the respective region. The regions were assumed to be uniform throughout the entire film thickness. The length of the filament was estimated from the 2D-XRD maps and the width of the filament was calculated by solving for W_{para-R} in Eq. (1) for a ρ_M and ρ_R of 0.16 Ω-cm and 2.8×10^{-4} Ω-cm, respectively, as determined from the ρ vs. *T* curve in Fig. 4(b)

$$R_{VO_2} = R_{series-M} + \left(\frac{R_{para-R}R_{para-M}}{R_{para-R}+R_{para-M}}\right)$$

$$R_{VO_2} = \frac{\rho_M L_{series-M}}{W_{series-M}t} + \left[\frac{\left(\frac{\rho_R L_{para-R}}{W_{para-R}t}\right)\left(\frac{\rho_M L_{para-M}}{W_{para-M}t}\right)}{\left(\frac{\rho_R L_{para-R}}{W_{para-R}t}\right)+\left(\frac{\rho_M L_{para-M}}{W_{para-M}t}\right)}\right]. \quad (1)$$

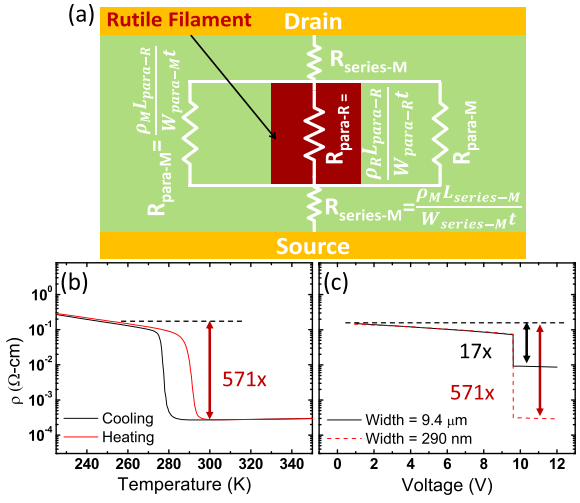

FIG. 4. (a) Illustration of the equivalent circuit used to calculate the filament width. (b) Temperature dependent resistivity of the VO_2 film for a thermally driven transition, showing a 571x change in resistivity. (c) (Black line) Bias dependent resistivity of the VO_2 device electrically driven from HRS to LRS, exhibiting only a 17x change in resistivity. (Dashed red line) Corrected bias dependent resistivity, with a reduced width of 290 nm after the transition to LRS, restoring the full magnitude of the resistivity change across the MIT.

TABLE I. Extracted R filament dimensions.

V	R Length (μm)	R Width (nm)	I (μA)	R_{VO_2} (kΩ)
0	0.5	50	…	95.6
8	3.2	200	92.0	49.0
10	6.0	270	227.8	5.9
12	6.0	290	275.9	5.5

When the transition to LRS occurs, the R filament length was set to the channel length and the $R_{series-M}$ term goes to zero. At 10 and 12 V, a filament width of 270 and 290 nm was determined, respectively; in excellent agreement with the experimental estimation of approximately 300 nm from the XRD intensity maps. A summary of the filament dimensions extracted from the X-ray imaging and Eq. (1) is shown in Table I. Figure 4(c) plots the extracted resistivity of the entire channel during an electrically driven transition. However, if considering only the 290 nm wide R-phase, the entire 571x resistivity change can be observed. These results emphasize the importance of understanding and quantifying the presence and dimensions of R filaments in the channel.

VO_2 has recently been demonstrated as an effective switching element in high density memory cells.[21] The memory cell exists as high or low load resistance, depending on its digital state, and understanding the role of R filament formation is critical for realizing ideal volume, write speeds, and performance for such a device. To quantify the effect of load resistance on VO_2 channel utilization, resistors from 3 k to 38 kΩ were placed in series with a 6 μm long channel of varying widths from 4 to 20 μm as illustrated in Fig. 5(a). All of the VO_2 devices and series resistor were biased at a fixed voltage $(18\,V = V_{VO_2} + V_{resistor})$ in the LRS. This ensures that the R filament length is fixed at the channel length (6 μm), so that the width can be extracted. The filament width was a function of series resistance, see Fig. 5(b). The device can be biased in such a way that either phase coexistence in the VO_2 channel or a complete transformation of the entire channel to the R phase is achieved. For the 3 kΩ load, a channel width up to approximately 17 μm can be fully utilized. By increasing the series resistance the decreasing current flow results in a smaller filament. This shows that for some given load resistance, a further increase in VO_2 channel width does not significantly decrease LRS resistance of the VO_2.

In-situ nanoscale X-ray mapping with resistivity measurements on VO_2 has revealed the formation of an R metallic filament in an insulating M1 film during an electrically driven MIT. This work also demonstrates that nanoscale R filaments comprising only a small portion of the total device area can exist in the VO_2 channel below biases required to switch to LRS, highlighting the importance of enhancing spatial resolution for the study of electrically driven phase transitions. The extracted filament size revealed that, depending on the load, the ratio of R/M1 phase can be externally controlled, which can have important implications on circuit designs using VO_2 to drive resistive loads.

The authors would like to thank Professor Srinivas Tadigadapa of Penn State Electrical Engineering for use of his wire bonder and Peter Schiffer at the University of Illinois for help with the transport measurements. We also wish to acknowledge useful discussions with Martin Holt of Argonne National Laboratory. Work at Argonne was supported by the U.S Department of Energy, Office of Science, Office of Basic Energy Sciences, under Contract No. DE-AC02-06CH11357. We acknowledge the financial support of the Office of Naval Research through Award N00014-11-1-0665 and the National Science Foundation through Award DMR-0820404.

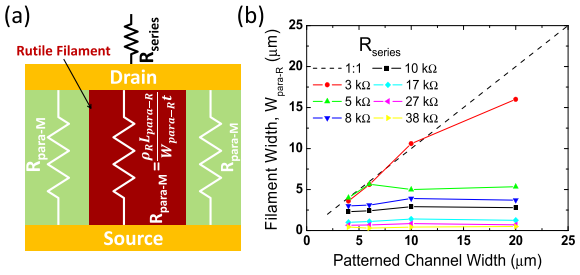

FIG. 5. (a) Circuit schematic overlaid on an illustration of the VO_2 channel in LRS with a resistor R_{series} in series. (b) The filament width dependence on the series resistor. At higher currents (lower series resistance), the whole channel width can be utilized as seen by the data points falling on the dashed line, representing a 1:1 relationship between the extracted and patterned filament width.

[1]F. Morin, Phys. Rev. Lett. **3**, 34 (1959).
[2]S. Jin, T. H. Tiefel, M. McCormack, R. A. Fastnacht, R. Ramesh, and L. H. Chen, Science **264**, 413 (1994).
[3]J. G. Bednorz and K. A. Müller, Z. Phys. B **64**, 189 (1986).
[4]J. H. Park, J. M. Coy, T. S. Kasirga, C. Huang, Z. Fei, S. Hunter, and D. H. Cobden, Nature **500**, 431 (2013).
[5]V. Eyert, Ann. Phys. **11**, 650 (2002).
[6]R. M. Wentzcovitch, Phys. Rev. Lett. **72**, 3389 (1994).
[7]C. Weber, D. D. ORegan, N. D. M. Hine, M. C. Payne, G. Kotliar, and P. B. Littlewood, Phys. Rev. Lett. **108**, 256402 (2012).
[8]K. Okazaki, H. Wadati, a. Fujimori, M. Onoda, Y. Muraoka, and Z. Hiroi, Phys. Rev. B **69**, 165104 (2004).
[9]S. Biermann, A. Poteryaev, A. Lichtenstein, and A. Georges, Phys. Rev. Lett. **94**, 026404 (2005).
[10]A. Belozerov, M. Korotin, V. Anisimov, and A. Poteryaev, Phys. Rev. B **85**, 045109 (2012).
[11]B.-J. Kim, Y. Lee, S. Choi, J.-w. Lim, S. Yun, H.-t. Kim, T.-J. Shin, and H.-S. Yun, Phys. Rev. B **77**, 235401 (2008).
[12]J. I. Sohn, H. J. Joo, D. Ahn, H. H. Lee, A. E. Porter, K. Kim, D. J. Kang, and M. E. Welland, Nano Lett. **9**, 3392 (2009).
[13]A. Zimmers, L. Aigouy, M. Mortier, A. Sharoni, S. Wang, K. West, J. Ramirez, and I. K. Schuller, Phys. Rev. Lett. **110**, 056601 (2013).
[14]J. Duchene, Appl. Phys. Lett. **19**, 115 (1971).
[15]J. Sakai and M. Kurisu, Phys. Rev. B **78**, 033106 (2008).
[16]T. Kanki, K. Kawatani, H. Takami, and H. Tanaka, Appl. Phys. Lett. **101**, 243118 (2012).
[17]H. Paik, J. Moyer, J. A. Mundy, J. Tashman, D. A. Muller, P. Schiffer, and D. G. Schlom, "Structure and transport property of ultrathin epitaxial VO_2 thin film on TiO_2 (001) substrate grown by MBE," (unpublished).
[18]D. B. McWhan, M. Marezio, J. P. Remeika, and P. D. Dernier, Phys. Rev. B **10**, 490 (1974).
[19]O. Madelung, M. Schulz, and H. Weiss, *Landolt-Börnstein: Numerical Data and Functional Relationships in Science and Technology, New Series, Group III* (Springer, 1984), Vol. 17g, p. 135.
[20]J. M. Wu and L. B. Liou, J. Mater. Chem. **21**, 5499 (2011).
[21]M.-J. Lee, Y. Park, D.-S. Suh, E.-H. Lee, S. Seo, D.-C. Kim, R. Jung, B.-S. Kang, S.-E. Ahn, C. Lee, D. Seo, Y.-K. Cha, I.-K. Yoo, J.-S. Kim, and B. Park, Adv. Mater. **19**, 3919 (2007).